analytical chemistry

Article

Cite This: *Anal. Chem.* 2019, 91, 7531−7537

pubs.acs.org/ac

# Self-Assembling Peptide-Based Multifunctional Nanofibers for Electrochemical Identification of Breast Cancer Stem-like Cells

Yingying Tang,[†] Yuhao Dai,[†] Xiang Huang,[‡] Lingling Li,[†] Bing Han,[†] Ya Cao,*[,†] and Jing Zhao*[,†]

[†]Center for Molecular Recognition and Biosensing, School of Life Sciences, Shanghai University, Shanghai 200444, P. R. China

[‡]Department of Oncology, The First Affiliated Hospital of Nanjing Medical University, Nanjing 210029, P. R. China

Supporting Information

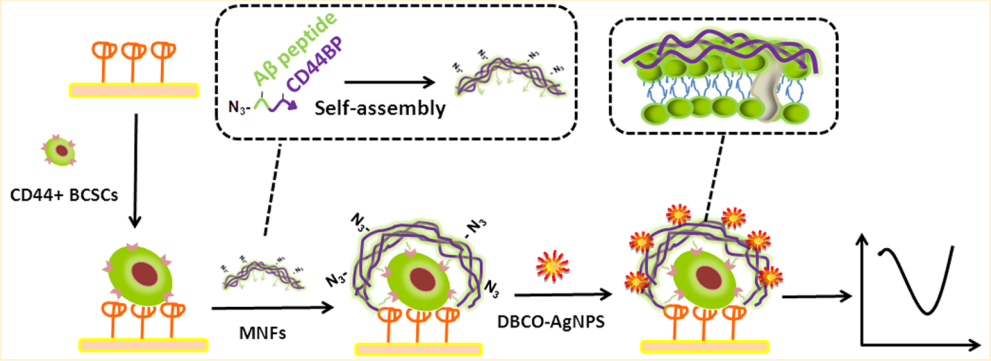


**ABSTRACT:** Cancer stem-like cells are closely related with the development and metastasis of tumors. Herein, an electrochemical method is proposed to identify stem-like cells in breast tumor. The core concept of the method is the use of multifunctional nanofibers (MNFs), which are synthesized through facile self-assembly of peptide probes. MNFs can perform three functions, specifically targeting surface biomarker to identify stem-like cells, recruiting silver nanoparticles (AgNPs) to generate electrochemical signals, and providing large amounts of reaction sites to amplify signals. Specially, breast cancer stem cells (BCSCs) are first captured by nucleolin aptamer immobilized on the electrode surface and then selectively recognized by MNFs through the binding with CD44, thereby offering a large number of azide groups for signal labeling. By tracing electrochemical signals from MNF-recruited AgNPs, the method demonstrates to detect target cells as low as 6 cells/mL within a wide linear range from 10 to $5 \times 10^5$ cells/mL. Moreover, the method can not only recognize BCSCs with high selectivity in complex environment but also monitor drug-induced stemness changes with high sensitivity, providing promising prospective clinic applications in the future.



In today's world, breast cancer is the most common malignant tumor among women. Although cure rate and survival rate have improved dramatically in recent decades, breast cancer is still a leading cause of death in females.[1−3] In 2003, Al-Hajj et al. discovered cancer stem cells (CSCs) in a breast tumor.[4] CSCs have self-renewal and differentiation capabilities as normal stem cells and are proven to be closely associated with increased tumor metastasis, relapse, and drug resistance.[5,6] Later, different biomarkers have been reported to indicate stem-like properties in breast cancer, revealing a high risk of metastatic disease and low overall survival in breast cancer patients, and also thus guiding diagnosis, treatment, and prognosis of breast cancer.[7−9] Lymphocyte receptor CD44 is the first established and most frequently used surface biomarker to identify stem-like properties in breast cells.[8] CD44 accounts for enhanced capabilities of tumor initiation and progression as well as epithelial-to-mesenchymal transition (EMT) for distant metastases.[10,11] CD44 is also a potential target for breast cancer therapy, which may eventually inhibit tumor development and reverse drug resistance through regulating self-renewal and maintenance of stem-like properties.[12−14] However, in spite of the finding of stemness markers, such as CD44, identification of stem-like cells in breast tumors always faces a big challenge in practice because the number of such cells is usually extremely low in real samples.

The latest advances in the field of peptide self-assembly may represent ideal opportunities to address aforementioned problems in the identification of stem-like cells. In living organisms, a huge quantity of noncovalent bonds act together to promote molecular self-assembly and subsequently maintain the advanced structure of biological macromolecules. Inspired by molecular self-assembly in vivo, biological molecules become appealing elements to fabricate diverse self-assembling nanostructures.[15−19] Among them, oligopeptide, a naturally occurring building block, is widely accepted in a controllable formation of a higher-order nanostructure that is usually driven

**Received:** November 19, 2018
**Accepted:** April 25, 2019
**Published:** April 25, 2019




DOI: 10.1021/acs.analchem.8b05359
*Anal. Chem.* 2019, 91, 7531−7537

**Scheme 1. Schematic Illustration of the Multifunctional Nanofiber-Assisted Electrochemical Identification of BCSCs**

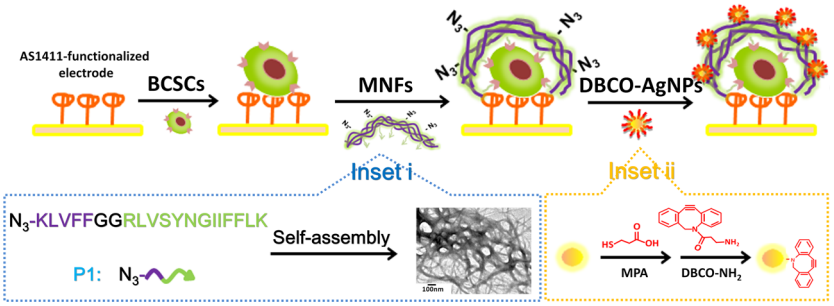


by intermolecular hydrogen bonds.[20−24] For example, short peptides derived from the amyloid beta peptide of Alzheimer's disease, such as dipeptides diphenylalanine FF and pentapeptide KLVFF, demonstrate the ability of spontaneous assembly into amyloid fibrils and thus prepare various nanostructures from nanofibers to nanoplates. These self-assembling peptide-based nanostructures not only provide enhanced surface area for increased accumulation of signal molecules but also are able to readily incorporate specific peptide domain to perform particular functions, thereby attracting increasing attention for biosensing applications.[25−27]

Taking the advantages of self-assembling peptide-based nanostructures, we herein propose an improved method to identify stem-like properties in breast cancer cells using sensitive electrochemical techniques.[28,29] As designed, breast stem cancer cells (BCSCs) are first captured on an electrode surface by nucleolin (NCL) aptamer AS1411 and then identified by self-assembling peptide-based multifunctional nanofibers (MNFs) that are able to selectively bind to stemness marker CD44. Subsequently, remarkable electrochemical signals are generated by recruiting electro-active silver nanoparticles (AgNPs) as labels. Experimental results reveal satisfactory sensitivity and selectivity of our method in distinguishing BCSCs, even in a complex environment, attributing to the utilization of MNFs for target recognition, signal labeling, and amplification at the same time.

## EXPERIMENTAL SECTION

**Chemicals and Materials.** DNA oligonucleotides used in this work were synthesized by Shanghai Sangon Biotech Co. Ltd., and their sequences are listed in Table S1. Peptide probes (P1, azide ($N_3$)-KLVFFGGRLVSYNGIIFFLK; P2, $N_3$-KLVFFGGVLFGFLKIYSRIN; and P3, $N_3$-RLVSYNGIIFFLK) were purchased from Zhejiang Ontores Biotechnologies Inc. Heparin sodium was purchased from Shenzhen Hepalink Pharmaceutical Group Co. Ltd. Silver nitrate ($AgNO_3$), trisodium citrate, sodium borohydride ($NaBH_4$), dibenzocyclooctyne-amine (DBCO-$NH_2$), mercaptohexanol (MCH), mercaptopropionic acid (MPA) and tris-(2-carboxyet-hyl) phosphine hydrochloride (TCEP) were obtained from Sigma-Aldrich. Fetal bovine serum (FBS) was purchased from Beijing Dingguo Changsheng Biotech Co. Ltd. MCF-7, HepG2, BT-474, and L02 cells were purchased from Shanghai Genechem Co. Ltd. DMEM, DMEM/F12, RPMI 1640, and B27 supplement were purchased from Gibco. EGF (epidermal growth factors) and bFGF (basic fibroblast growth factors) were purchased from Peprotech Inc. DBCO-Cy5 was purchased from Xian Ruixi Biological Technology Co. Ltd. Anti-NCL/FITC was purchased from Beijing Biosynthesis Biotechnology Co. Ltd. Anti-CD44/FITC was purchased from Thermo Fisher Scientific Inc. Aptamer immobilization buffer was 10 mM Tris-HCl (pH 7.4) containing 1 mM EDTA, 0.1 M NaCl, and 1 mM TCEP; electrolyte solution for electrochemical impedance spectra (EIS) was 0.1 M PBS (pH 7.4) containing 5 mM $Fe(CN)_6^{3-/4-}$; and electrolyte solution for linear sweep voltammetry (LSV) was 0.1 M PBS (pH 7.4) containing 0.1 M KCl.

**Preparation of AS1411-Functionalized Electrode.** The substrate gold electrode was carefully polished to a mirror-like smooth by using 1, 0.3, and 0.05 $\mu$m alumina slurry, respectively. Then, gold electrode was covered by piranha solution ($H_2SO_4/H_2O_2$= 3:1) for 5 min, which was ultrasonicated in both doubly distilled water and ethanol for 5 min, respectively. Finally, the polished electrode was electrochemically cleaned in 0.5 M $H_2SO_4$ by scanning from 0 to 1.5 V to remove the impurities. After being dried in the nitrogen atmosphere, the cleaned electrode was immersed into the immobilization buffer containing 2 $\mu$M AS1411 aptamer for 16 h, which was then treated with 1 mM MCH for 30 min. After being thoroughly washed by doubly distilled water, the AS1411-functionalized electrode was prepared to capture BCSCs. The surface density was estimated as $3.03 \times 10^{11}$ molecules/cm$^2$ by using chronocoulometric measurements.[30]

**Cell Culture and Capture.** MCF-7, HepG2, and BT-474 cells were grown in DMEM with 10% FBS, while L02 cells were grown in RPMI 1640 with 10% FBS. All cell lines were grown in a humidified atmosphere (5% $CO_2$) at 37 °C. BCSCs were enrichment by serum-free culture. After being cultured for 72 h, MCF-7 cells were harvested at the end of the log phase using 0.25% trypsin digestion, followed by centrifugation at 500 rpm for 5 min to separate from the supernatant. Then, the cells were incubated in DMEM/F12 with the addition of 10 ng/mL of bFGF, 20 ng/mL of EGF, and 0.4% B27. When BCSCs were enriched in the form of suspended microspheres, they were detached by trypsin digestion and dispersed in a sterile PBS containing 1 mM $Ca^{2+}$ and 1 mM $Mg^{2+}$. After being harvested, the BCSCs were incubated with the AS1411-functionalized electrode at room temperature for 2 h. For control experiments, HepG2, BT-474, and L02 cells were used instead of BCSCs.

**Preparation of DBCO-Functionalized AgNPs (DBCO-AgNPs).** AgNPs were prepared based on a previous report.[31] In brief, 6 mL of 5 mM $NaBH_4$ was added drop-by-drop to 100 mL of a mixture of 0.25 mM $AgNO_3$ and 0.25 mM trisodium citrate under vigorous stirring for 30 min. When the color of the solution gradually changed to yellow, the obtained solution was kept in dark overnight. For the functional modification, 1 mM MPA was added into 1 mL of AgNPs for 16 h at 4 °C, so the carboxyl group was attached on the surface of AgNPs through silver−sulfur interaction. After that, 1 mM DBCO-


DOI: 10.1021/acs.analchem.8b05359
Anal. Chem. 2019, 91, 7531−7537

$NH_2$ was added to obtain DBCO-AgNPs through interaction of the carboxyl and amino groups.

**Electrochemical Identification of BCSCs by Using Self-Assembling Peptide-Based MNFs.** To obtain self-assembling MNFs, 100 $\mu$M P1 was incubated at 37 °C for 2 h. After that, the cell-captured electrode was reacted with self-assembling MNFs for 2 h at room temperature. Then, the prepared DBCO-AgNPs were bound to MNFs through click chemistry-assisted linkage for 1 h at 25 °C. After being rinsed with doubly distilled water, the electrode was used for electrochemical measurements, which were carried out on a model 660c Electrochemical Analyzer (CH Instruments). A three-electrode system was used, consisting of a modified gold electrode, a saturated calomel electrode (SCE), and a platinum wire electrode. EIS was obtained with a biasing potential of 0.224 V, amplitude of 5 mV, and a frequency range from 1 Hz to 100 kHz. LSV was performed by scanning from −0.2 to 0.3 V at a rate of 100 mV/s.

## RESULTS AND DISCUSSION

**Strategy for Electrochemical Identification of BCSCs.** The strategy for electrochemical identification of BCSCs is illustrated in Scheme 1. Three components are involved in the procedure, including the AS1411-functionalized electrode, self-assembling peptide-based MNFs, and DBCO-AgNPs. Inset i describes fabrication of MNFs via self-assembly of peptide probes. Specifically, peptide probe P1 includes three modules, (1) the $N_3$ group at the N-terminal for ligation with DBCO-AgNPs, (2) the KLVFF peptide motif for controllable formation of $\beta$-sheet structured nanofibers,[32] and (3) the CD44 binding peptide (CD44BP) motif for stemness recognition.[33] Under routine condition, P1 self-assembles to $\beta$-sheet-structured MNFs by making use of the KLVFF motif thus, a large number of azide groups are exposed on MNF surfaces for signal labeling and amplification. Inset ii displays preparation of DBCO-AgNPs, which is used as a remarkable source of detectable signal in electrochemical analysis. After the preparation of MNFs and DBCO-AgNPs, the identification of BCSCs is realized by using CD44 as a representative stemness marker. As illustrated, the AS1411 aptamer, an FDA approved DNA aptamer, is first immobilized on the electrode surface through Au−S interaction, which can capture BCSCs by binding overexpressed NCL on the cell surface.[34] Then, MNFs selectively recognize and bind to BCSCs by making use of the binding motif. Compared to the conventional antibody, CD44BP has unique advantages of simple synthesis, low cost, high resistance to harsh environments, and high flexibility for engineering at the molecular level, which is also superior to the native ligand of CD44 hyaluronic acid (HA) when binding to cancer cells. After that, a large amount of azide groups at MNF surfaces triggers ligation with DBCO-AgNPs smoothly through click chemistry, and thus contributes to an amplified electrochemical signal from surface-attached AgNPs. Overall, BCSCs can be effectively determined by tracing silver responses with the use of a multifunctional platform.

**Characterization of Self-Assembling Peptide-Based MNFs.** Deemed to be the core component of the method, the preparation and usability of self-assembling peptide-based MNFs was first characterized. The TEM image in Figure S1A shows a long fibrous bundle morphology of MNFs, confirming good self-assembling performance of P1. The $\beta$-sheet structure of MNFs was then confirmed by a positive circular dichroism (CD) signal at around 205 nm and a positive one at around 218 nm (Figure S1B).[32] Figure 1 exhibits fluorescent images of BCSCs following incubation with MNFs. Obviously, by using

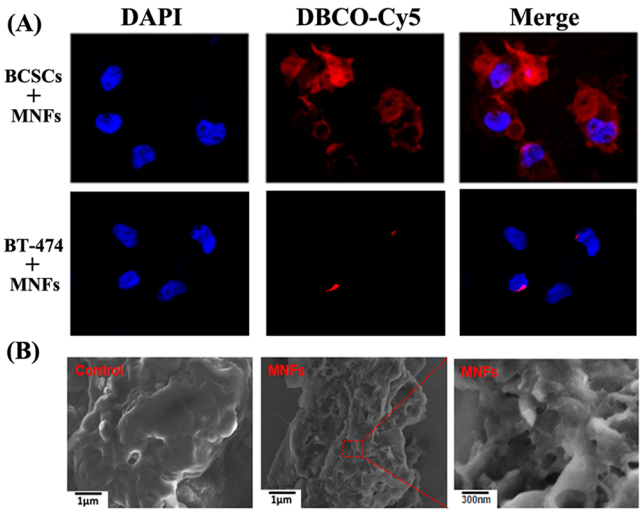


**Figure 1.** (A) Fluorescence microscope images of BCSCs and control cells (BT-474 cells as the model) following incubation with MNFs. (B) SEM images of BCSCs surface (control) and those after being treated with MNFs.

DBCO-Cy5 as a fluorescent dye, a fibrous network was shown to surround a large surface area of BCSCs with a quite strong red fluorescence, not only confirming the presence of azide groups on MNFs surface but also demonstrating a favorable performance of MNFs for BCSC recognition and signal labeling. However, once MNFs were incubated with CD44-negative control cells (e.g., BT-474 cells), nearly no fluorescent signals could be observed in the presence of DBCO-Cy5, further demonstrating the ability of MNFs to selectively identify stemness biomarkers of breast cancer cells. SEM also demonstrated the interaction of MNFs and surface-immobilized BCSCs. Figure 1B displays SEM observation of the morphological changes at a gold surface. BCSCs were captured on the gold surface through binding with the AS1411 aptamer, showing a relatively smooth cell membrane with some irregular protrusions (left in Figure 1B). After MNFs bound to the surface of a captured cell through CD44 recognition, a fibrous network was observed to surround the cell surface with improved surface roughness (middle and right in Figure 1B). Overall, the imaging results well demonstrated stemness identification of MNFs on the surface of BCSCs.

**EIS Studies of BCSCs Capture and Recognition at a Gold Electrode.** In order to prove surface capture and stemness recognition of BCSCs at a gold electrode, an electrochemical technique EIS was first utilized. Figure 2A shows a schematic illustration of a stepwise modification at a gold electrode, and Figure 2B shows the corresponding EIS results. Nearly no impedance was observed at a bare gold electrode, which was ascribed to a feasible approach of $Fe(CN)_6^{3-/4-}$ to the electrode surface (curve a). Gradual increases of impedance values were obtained after aptamer functionalization (curve b) and following BCSC capture (curve c), and a rapid rise of the impedance was observed after incubating surface-captured cells with MNFs (curve d). EIS results are quite reasonable based on our principle. The immobilization of the AS1411 aptamer increased negative charges on the electrode surface, thereby electrostatically


DOI: 10.1021/acs.analchem.8b05359
Anal. Chem. 2019, 91, 7531−7537

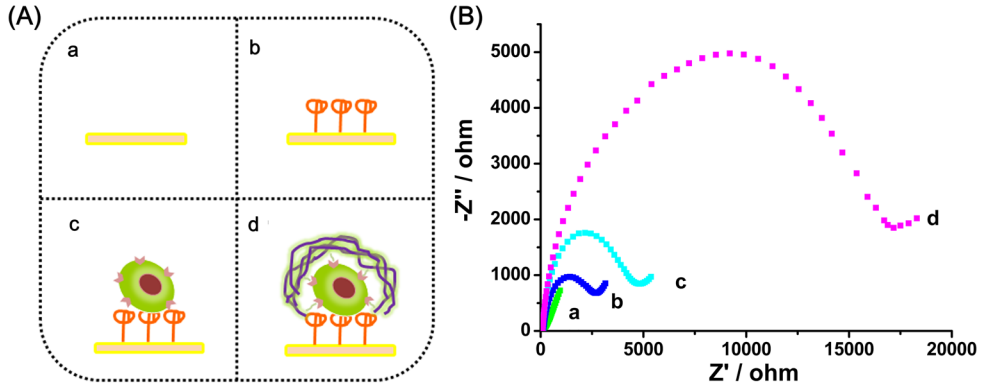


**Figure 2.** (A) Schematic illustration and (B) corresponding EIS results of stepwise changes at a gold electrode. (a) Bare gold electrode, (b) AS1411-functionalized electrode, (c) AS1411-functionalized electrode incubated with BCSCs, and (d) AS1411-functionalized electrode incubated with BCSCs and MNFs in sequence.

repelling $Fe(CN)_6^{3-/4-}$. When BCSCs were captured on the electrode surface after interaction with the AS1411 aptamer, enhanced steric hindrance further prohibited the approach of electro-active species to the electrode surface. This could also be verified by a positive correlation between the impedance change and the coverage of the cells (Figure S2A). When MNFs bound to BCSC surfaces through the CD44BP motif, the large-sized nanofiberous network induced a great steric effect for serious prohibition of electron transfer to the electrode, leading to a dramatic increase of the impedance value. In addition to BSCSs, BT-474 cells were also tested as a control. It can be seen from Figure S2B, that BT-474 cells were also captured on the electrode surface because of their expression of NCL, which produced an increased impedance value (Figure S2B, curve c). However, nearly no impedance change could be further observed (Figure S2B, curve d), revealing unsuccessful recruitment of MNFs and indicating the selectivity of MNF-based stemness identification. Moreover, control experiments were performed using a random DNA instead of the AS1411 aptamer or simultaneously using the AS1411 aptamer and its complementary DNA. As shown in Figure S2C,D, BCSCs could not be captured on the electrode surface in both cases, which confirmed that the capture of BCSCs was realized under the action of the AS1411 aptamer. Overall, EIS studies clearly demonstrated feasibility of our principle for step-by-step surface reaction and molecular recognition at a gold electrode.

**LSV Studies of MNF-Assisted Signal Labeling and Amplification for BCSCs Identification.** After confirmation of the BCSC capture and recognition at a gold electrode by EIS, another electrochemical technique, LSV, was utilized to demonstrate MNF-assisted signal labeling. Figure 3A displays electrochemical responses of a gold electrode at different cases. A quite high electrochemical response was observed after linkage of MNFs and DBCO-AgNPs on surface-captured BCSCs in sequence (curve a), while an extremely low electrochemical response was observed in the absence of BCSCs (curve b). The comparison confirmed that electrochemical signal was attributed to DBCO-AgNPs that were labeled on MNFs recruited by BCSCs. In detail, when BCSCs were captured on the AS1411-funcationalized electrode, MNFs recognized and bound to CD44 on BCSCs, providing sufficient reaction sites ($N_3$ groups). Then, DBCO-AgNPs were labeled on MNFs through the well-known click chemistry between DBCO groups and $N_3$ groups and then served as the signal

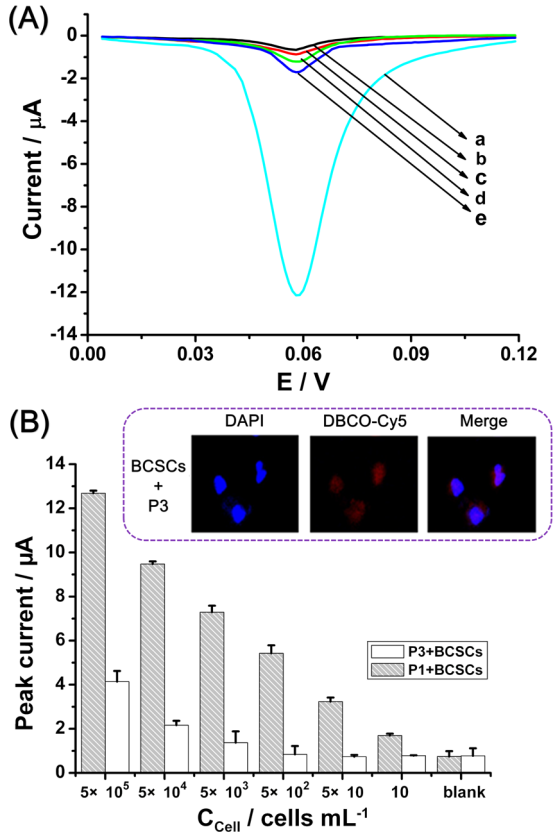


**Figure 3.** (A) LSV responses obtained at the AS1411-functionalized electrode in the presence of BCSCs (curve a) or in the absence of BCSCs (curve b), or after the capture of BCSCs in the presence of bare AgNPs (curve c), in the presence of P2 (curve d), or in the presence of heparin (curve e). (B) Corresponding electrochemical quantitative analysis using P1 and P3. Inset shows fluorescence microscope images of BCSCs following incubation with P3.

source to produce significant electrochemical response. By contrast, once BCSCs did not exist, the MNFs could not be recruited to the electrode surface and thus failed to mediate the labeling of DBCO-AgNPs, resulting in negligible electrochemical response. In addition, control experiment revealed that bare AgNPs were not able to be labeled on MNFs for the lack of DBCO groups, which led to an extremely low electrochemical response (curve c). These data clearly verified


DOI: 10.1021/acs.analchem.8b05359
Anal. Chem. 2019, 91, 7531−7537

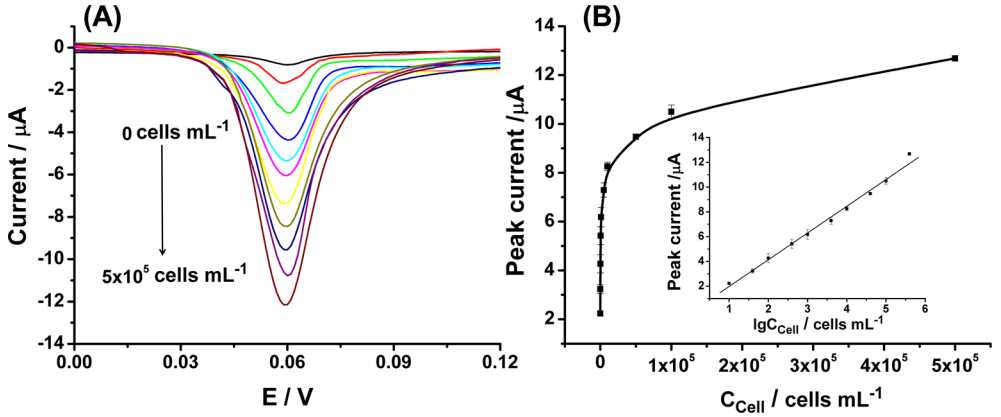


**Figure 4.** (A) Electrochemical responses obtained with different concentrations of BCSCs from 0 to 5 × $10^5$ cells/mL. (B) The peak currents obtained in the presence of different concentrations of BCSCs. Inset shows a linear relationship between peak current and the logarithm of BCSCs concentration from 10 to 5 × $10^5$ cells/mL. Error bars represent the standard deviations of three independent measurements.

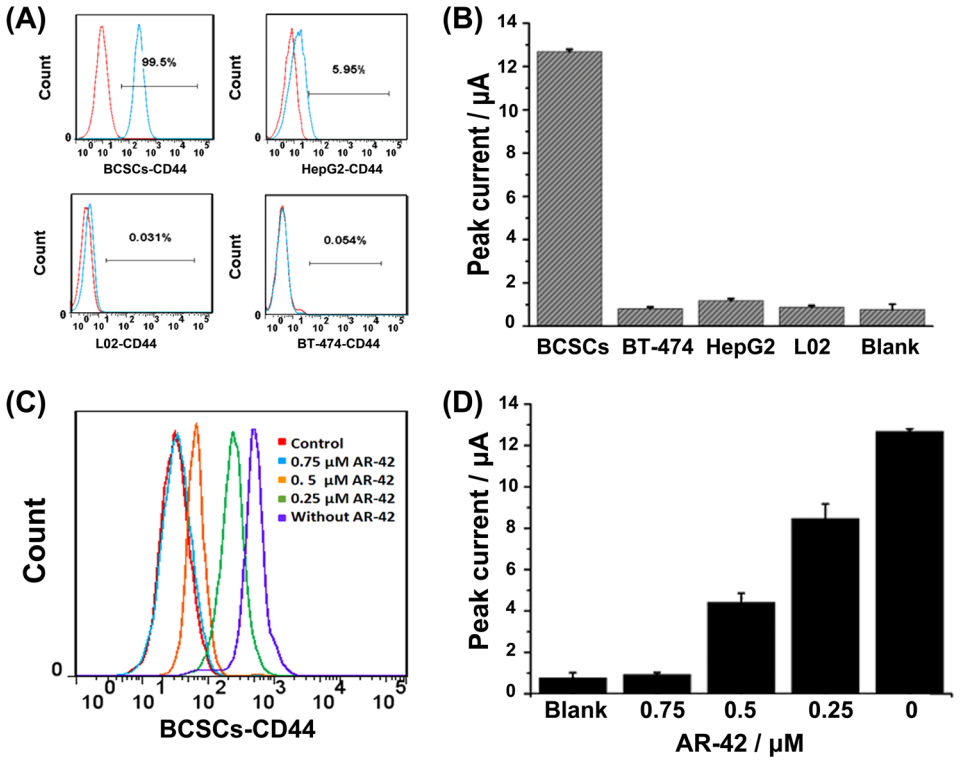


**Figure 5.** (A) Flow cytometry assay of CD44 expression in different cells. (B) The peak current obtained in the presence of different cells. The concentrations of cells are 5 × $10^5$ cells/mL. (C) Flow cytometry assay of CD44 expression on BCSCs after treatment with different concentrations of AR-42. (D) Corresponding electrochemical responses of BCSCs after AR-42 treatment.

the function of MNFs in signal labeling for their possession of a large number of $N_3$ groups.

Fluorescence imaging and EIS experiments revealed the ability of MNFs to selectively identify stem-like breast cancer cells, which was presumed to be derived from the CD44-targeting capability of the CD44BP motif. To provide a deeper insight into this inspiring nature, a control peptide probe P2 was designed by replacing the CD44BP motif with a random sequence. As shown in Figure 3A, a quite low electrochemical response was obtained when using P2 as probes (curve d). Clearly, although P2 contained the self-assembling motif for fibrous self-assembly and the azide group for the signal labeling, the lack of the CD44BP motif prohibited the binding of nanofibers to BCSCs. This indicated the critical role of the CD44BP motif in the stemness identification of MNFs. In addition, heparin, a competitive inhibitor of the CD44 binding ligand, was also used.[35] As expected, a decreased electrochemical response was obtained because competitive inhibition breached the interaction between the CD44BP motif and CD44, which prevented MNFs from being recruited onto BCSCs (Figure 3A, curve e). Overall, these results validated that MNF-based stemness identification relied on the specific interaction of the CD44BP motif and the surface biomarker CD44.

To verify the signal amplification function of MNFs, we designed another control peptide, P3, an azide group-modified CD44BP. Compared to P1, P3 is unable to initiate fibrous formation for the lack of the self-assembling motif. Figure 3B


DOI: 10.1021/acs.analchem.8b05359
Anal. Chem. 2019, 91, 7531−7537

shows LSV peak currents obtained in the presence of different concentrations of BCSCs when using MNFs or P3 as probes. Obviously, peak currents in the presence of MNFs increased with the BCSC concentration in the range of 10−5 × $10^5$ cells/mL, and stem-like cancer cells could be easily distinguished even at a low concentration of 10 cells/mL (gray columns). In contrast, although P3 could bind to CD44 and induced electrochemical response from the click chemistry-assisted signal labeling, peak currents for P3-treated BCSCs, which also increased with BCSC concentrationa ranging from 5 × $10^2$ to 5 × $10^5$ cells/mL, were all much lower than those using MNFs, and only a slight increase of electrochemical signal was observed at a relatively high concentration of 500 cells/mL (white columns). The results were in good agreement with fluorescence studies. For fluorescent images, only a few red spots were scattered on the surfaces of BCSCs after P3 treatment, as shown in the inset of Figure 3B. Therefore, the comparison indicated that MNFs as an aggregate of P1 were able to provide enhanced reaction sites for AgNP loading compared to single CD44BP, thereby contributing to the high efficiency of signal amplification even at an ultralow concentration.

**Sensitivity of BCSCs Identification Using MNFs.** We optimized different experimental conditions to ensure high sensitivity of our method. Figure S3 shows peak currents under different self-assembly conditions. The formation of MNFs demonstrated to be both time- and concentration-dependent, suggesting an optimized time and concentration of 2 h and 100 $\mu$M. Figure S4 shows peak currents with different concentrations of AS1411 aptamers for modification of a gold electrode, providing the optimized concentration of 2 $\mu$M. Figure S5 shows a peak current with a different reaction time of the binding of MNFs and BCSCs, indicating the optimized reaction time of 1.5 h. Under optimized conditions, Figure 4A further displays electrochemical responses with the addition of different concentrations of target cells. Peak currents from surface-attached AgNPs gradually increased with the addition of BCSCs, suggesting an increased amount of surface-attached MNFs upon recognition and binding of the stemness marker. Figure 4B further reveals the relationship between the absolute value of peak current and BCSC concentrations. The absolute value of peak current increased linearly with the logarithmic value of cell concentration in the range of 10−5 × $10^5$ cells/mL. The regression equation is $|I|$ ($\mu$A) = −0.018 + 0.216 lgC (cells/mL), $R^2$ = 0.994. The limit of detection (LOD) is calculated to be 6 cells/mL (defined as a signal-to-noise ratio of three), presenting an improved sensitivity compared to the existing methods.[36,37] Moreover, relative standard deviations (RSDs) for repeated measurements were all within 10%, and the average of the RSDs was 4.19%, implying quite good reproduction of our methods.

**Specificity of BCSCs Identification Using MNFs.** To demonstrate high specificity of our method, electrochemical responses were studied using different cells as controls. Figure 5A shows the flow cytometry assay of CD44 expression in different cells. CD44 expression was 99.5, 5.59, 0.054, and 0.031% for BCSCs, HepG2, BT-474, and L02, respectively. Figure 5B displays electrochemical responses in the presence of different cells. A quite high peak current was observed with the addition of BCSCs, while only quite low electrochemical responses were observed with the addition of control cells, which approached the background signals. Although the cells may have a comparable expression of NCL (shown in Figure S6), only selective recognition of the stemness marker CD44 could activate multiple signal labeling and amplification for electrochemical analysis, demonstrating high specificity of our method. In addition, considering the electrochemical response was obtained based on the simultaneous expression of CD44 and NCL, double-staining flow cytometry analysis was performed to examine the distribution of different cells. As shown in Figure S7, the percentages of both CD44- and NCL-positive cells are quite consistent with the electrochemical results. To evaluate the performance of our method in a complex environment, different amounts of BCSCs were added to serum samples instead of buffer. Figure S8 compares peak currents of BCSCs in the buffer with that in serum samples. Electrochemical responses in the serum samples were quite comparable to that in the buffer, which clearly reconfirmed satisfactory specificity of our method even in a complex environment. Therefore, our method may have great potentials for practical applications in clinical diagnosis and cell classifications in the future.

AR-42, a novel deacetylase inhibitor, is able to reduce CD44 expression through down-regulation of the RNA binding protein IGF2BP3 that physically binds to CD44 mRNA to increase its stability.[38] In this work, we used AR-42 to down-regulate CD44 expression and then analyzed CD44 expression of BCSCs using our method. The suppressive effect on CD44 expression was first confirmed by flow cytometry. Figure 5C displays flow cytometry analysis of CD44 expression in BCSCs after treatment with different concentrations of AR-42. The CD44 expression was found to be 0.021, 8.92, 80.6, and 99.8% for 0.75, 0.5, 0.25, and 0 $\mu$M AR-42, respectively. Figure 5D further reveals corresponding electrochemical responses after treatment of BCSCs with different concentrations of AR-42. As expected, peak currents were found to decrease with an increase of AR-42 concentration, which was in good agreement with flow cytometry assay. Down-regulation of CD44 expression reduced the binding sites for MNFs, thereby inhibiting the production of electrochemical responses. Overall, electrochemical results of inhibitory effects not only verified the usability of our method in monitoring drug-induced stemness changes in clinical treatment but also suggested its potential application in drug development for cancer therapy in the future.

## CONCLUSION

Design and preparation of a particular nanostructured material, especially a self-assembling peptide-based nanostructure, have attracted increasing attention for its excellent performance in molecular recognition and signal amplification. In this work, we prepared a multifunctional peptide probe that could meet the requirement of molecular self-assembly, target recognition, and signal amplification at the same time. The binding peptide that was easily incorporated in the design of the peptide probe promoted the identification of a stemness biomarker in breast cancer cells, while self-assembled nanofibers provided increased binding sites for largely enhanced electrochemical signals. By mutual authentication of electrochemical studies with fluorescent analysis, our methods demonstrated high sensitivity and selectivity toward analysis of BCSCs by using MNFs. Given that accurate identification of BCSCs and down-regulation of cancer stemness have been proven in a complex environment, our method suggests great potential in clinical diagnosis and treatment of breast cancer. Accordingly, our method may have extensive use in tumor classification and


DOI: 10.1021/acs.analchem.8b05359
Anal. Chem. 2019, 91, 7531−7537

drug development only by changing the design of the binding ligand motif.

## ■ ASSOCIATED CONTENT

### Supporting Information

The Supporting Information is available free of charge on the ACS Publications website at DOI: 10.1021/acs.analchem.8b05359.

Sequences of DNA oligonucleotides used in this work, TEM image and CD spectrum of self-assembled MNFs, EIS results corresponding to a series of control experiments, optimization of P1 concentration and reaction time for the preparation of self-assembled MNFs, optimization of concentration of AS1411 aptamer, optimization of reaction time between self-assembled MNFs and BCSCs, flow cytometry assay of NCL expression on different cells, flow cytometry analysis of various cell lines with double-staining for CD44 and NCL, and peak currents obtained in different concentrations of BCSCs in serum and buffer (PDF)

## ■ AUTHOR INFORMATION


### Corresponding Authors

*E-mail: conezimint@shu.edu.cn.
*E-mail: jingzhao@t.shu.edu.cn.

### ORCID

Jing Zhao: 0000-0001-6424-3085


### Notes

The authors declare no competing financial interest.

## ■ ACKNOWLEDGMENTS

This work was supported by the National Natural Science Foundation of China (Grants 81671781, and 81871449).

## ■ REFERENCES


(1) DeSantis, C. E.; Ma, J.; Goding Sauer, A.; Newman, L. A.; Jemal, A. *Ca-Cancer J. Clin.* **2017**, *67*, 439−448.
(2) Mittal, S.; Kaur, H.; Gautam, N.; Mantha, A. K. *Biosens. Bioelectron.* **2017**, *88*, 217−231.
(3) Nagata, T.; Shimada, Y.; Sekine, S.; Hori, R.; Matsui, K.; Okumura, T.; Sawada, S.; Fukuoka, J.; Tsukada, K. *Breast Cancer.* **2014**, *21*, 96−101.
(4) Al-Hajj, M.; Wicha, M. S.; Benito-Hernandez, A.; Morrison, S. J.; Clarke, M. F. *Proc. Natl. Acad. Sci. U. S. A.* **2003**, *100*, 3983−3988.
(5) Qin, H.; Zhao, C.; Sun, Y.; Ren, J.; Qu, X. *J. Am. Chem. Soc.* **2017**, *139*, 16201−16209.
(6) Dontu, G.; Al-Hajj, M.; Abdallah, W. M.; Clarke, M. F.; Wicha, M. S. *Cell Proliferation* **2003**, *36*, 59−72.
(7) Wright, M. H.; Calcagno, A. M.; Salcido, C. D.; Carlson, M. D.; Ambudkar, S. V.; Varticovski, L. *Breast Cancer Res.* **2008**, *10*, R10.
(8) Olsson, E.; Honeth, G.; Bendahl, P. O.; Saal, L. H.; Gruvberger-Saal, S.; Ringnér, M.; Vallon-Christersson, J.; Jönson, G.; Holm, K.; Lövgren, K.; et al. *BMC Cancer* **2011**, *11*, 418.
(9) Ricardo, S.; Vieira, A. F.; Gerhard, R.; Leitão, D.; Pinto, R.; Cameselle-Teijeiro, J. F.; Milanezi, F.; Schmitt, F.; Paredes, J. *J. Clin. Pathol.* **2011**, *64*, 937−946.
(10) Yang, X.; Zhou, R.; Hao, Y.; Yang, P. *Sci. Bull.* **2017**, *62*, 923−930.
(11) Bowerman, C. J.; Nilsson, B. L. *J. Am. Chem. Soc.* **2010**, *132*, 9526−9527.
(12) He, L.; Gu, J.; Lim, L. Y.; Yuan, Z. X.; Mo, J. *Front. Pharmacol.* **2016**, *7*, 313.
(13) Liang, D. S.; Zhang, W. J.; Wang, A. T.; Su, H. T.; Zhong, H. J.; Qi, X. R. *Biomaterials* **2017**, *137*, 23−36.
(14) Yan, Y.; Zuo, X.; Wei, D. *Stem Cells Transl. Med.* **2015**, *4*, 1033−1043.
(15) Lin, T.; Yan, J.; Ong, L. L.; Robaszewski, J.; Lu, H. D.; Mi, Y.; Yin, P.; Wei, B. *Nano Lett.* **2018**, *18*, 4791−4795.
(16) Shao, Y.; Jia, H.; Cao, T.; Liu, D. *Acc. Chem. Res.* **2017**, *50*, 659−668.
(17) Zhang, S.; Zhang, J.; Fang, W.; Zhang, Y.; Wang, Q.; Jin, J. *Nano Lett.* **2018**, *18*, 6563−6569.
(18) Sun, H.; Luo, Q.; Hou, C.; Liu, J. *Nano Today* **2017**, *14*, 16−41.
(19) Mao, X.; Chen, G.; Wang, Z.; Zhang, Y.; Zhu, X.; Li, G. *Chem. Sci.* **2018**, *9*, 811−818.
(20) Wei, G.; Su, Z.; Reynolds, N. P.; Arosio, P.; Hamley, I. W.; Gazit, E.; Mezzenga, R. *Chem. Soc. Rev.* **2017**, *46*, 4661−4708.
(21) Nambiar, M.; Wang, L. S.; Rotello, V. M.; Chmielewski, J. *J. Am. Chem. Soc.* **2018**, *140*, 13028−13033.
(22) Frederix, P. W.; Scott, G. G.; Abul-Haija, Y. M.; Kalafatovic, D.; Pappas, C. G.; Javid, N.; Hunt, N. T.; Ulijn, R. V.; Tuttle, T. *Nat. Chem.* **2015**, *7*, 30−37.
(23) Zhang, W.; Yu, X.; Li, Y.; Su, Z.; Jandt, K. D.; Wei, G. *Prog. Polym. Sci.* **2018**, *80*, 94−124.
(24) Fan, Z.; Sun, L. M.; Huang, Y. J.; Wang, Y. Z.; Zhang, M. J. *Nat. Nanotechnol.* **2016**, *11*, 388−394.
(25) Li, S.; Zou, R.; Tu, Y.; Wu, J.; Landry, M. P. *Chem. Sci.* **2017**, *8*, 7552−7559.
(26) Vigier-Carrière, C.; Wagner, D.; Chaumont, A.; Durr, B.; Lupattelli, P.; Lambour, C.; Schmutz, M.; Hemmerlé, J.; Senger, B.; Schaaf, P.; Boulmedais, F.; Jierry, L. *Langmuir* **2017**, *33*, 8267−8276.
(27) Zhao, J.; Yang, L.; Dai, Y.; Tang, Y.; Gong, X.; Du, D.; Cao, Y. *Biosens. Bioelectron.* **2018**, *119*, 42−47.
(28) Ciui, B.; Tertis, M.; Cernat, A.; Sandulescu, R.; Wang, J.; Cristea, C. *Anal. Chem.* **2018**, *90*, 7761−7768.
(29) Ciui, B.; Tertis, M.; Feurdean, C. N.; Ilea, A.; Sandulescu, R.; Wang, J.; Cristea, C. *Sens. Actuators, B* **2019**, *281*, 399−407.
(30) Steel, A. B.; Herne, T. M.; Tarlov, M. J. *Anal. Chem.* **1998**, *70*, 4670−4677.
(31) Miao, P.; Tang, Y. G.; Yin, J. *Chem. Commun.* **2015**, *51*, 15629−15632.
(32) Yang, P. P.; Luo, Q.; Qi, G. B.; Gao, Y. J.; Li, B. N.; Zhang, J. P.; Wang, L.; Wang, H. *Adv. Mater.* **2017**, *29*, 1605869.
(33) Zhao, J.; Tang, Y.; Cao, Y.; Chen, T.; Chen, X.; Mao, X.; Yin, Y.; Chen, G. *Electrochim. Acta* **2018**, *283*, 1072−1078.
(34) Fonseca, N. A.; Cruz, A. F.; Moura, V.; Simões, S.; Moreira, J. N. *Crit. Rev. Oncol. Hematol.* **2017**, *113*, 111−121.
(35) Golan, M.; Feinshtein, V.; Polyak, D.; Scomparin, A.; Satchi-Fainaro, R.; David, A. *Bioconjugate Chem.* **2016**, *27*, 947−960.
(36) Roberts, W. S.; Davis, F.; Holmes, J. L.; Collyer, S. D.; Larcombe, L. D.; Morgan, S. L.; Higson, S. P. *Biosens. Bioelectron.* **2013**, *41*, 282−288.
(37) Jeong, H. Y.; Baek, S. H.; Chang, S. J.; Cheon, S. A.; Park, T. J. *Colloids Surf., B* **2015**, *135*, 309−315.
(38) Canella, A.; Nieves, H. C.; Sborov, D. W.; Cascione, L.; Radomska, H. S.; Smith, E.; Stiff, A.; Consiglio, J.; Caserta, E.; Rizzotto, L.; et al. *Oncotarget.* **2015**, *6*, 31134.




DOI: 10.1021/acs.analchem.8b05359
*Anal. Chem.* 2019, 91, 7531−7537